NOTES AND CORRESPONDENCE

Effects of Stratification on Surface Frontogenesis: Warm and Cold Fronts

PETER R. BANNON

Department of the Geophysical Sciences, The University of Chicago, Chicago, IL 60637

9 December 1983 and 9 April 1984

ABSTRACT

The role of the ambient stratification in semigeostrophic surface frontogenesis is examined. Model fronts forming in regions of large static stability 1) are weaker, 2) are tilted more toward the horizontal, and 3) propagate more slowly toward the warm air than fronts forming in regions of small static stability.

These results are discussed in light of the differences between warm and cold fronts.

1. Introduction

The Bergen school of meteorology contributed the distinction between warm and cold fronts. Earlier investigators (e.g., see Palmén and Newton, 1969; Kutzbach, 1979) had documented the cold front, but the warm front was identified only after careful synoptic analysis at Bergen (Bjerknes, 1919).

Warm and cold fronts differ in their directions and speeds of propagation, their vertical structures, their strengths, and their cloud patterns. The difference in their directions of propagation defines warm fronts from cold fronts. Typically, cold fronts propagate faster than warm fronts (Gidel, 1978), and this behavior is consistent with the occlusion process. While the frontal surface of both fronts extends from the ground and tilts in the vertical to lie over the cold air, cold fronts have slopes (1:50–150) roughly twice those of warm fronts (Byers, 1974). The not uncommon difficulty of locating the warm front associated with a surface low suggests that warm fronts are weaker than cold fronts. The Bjerknes and Solberg (1921, 1922) cyclone model exhibits widespread pre-warm-frontal stratus clouds, compared to pre-cold-frontal cumulus clouds. Subsequent investigators (for a review see, e.g., Houze and Hobbs, 1982) have refined this model to include rainbands, but the difference in cloud type remains. It should be emphasized that, although synoptic experience suggests these distinctions, statistical documentation is unavailable in the literature.

The earliest dynamical explanation of these differences stressed the observed variation in the direction of propagation. Bergeron (1937) argued that in the presence of surface friction this difference would lead to steep cold fronts and gradually-sloping warm fronts. Ball (1960) presented an analytic model of this effect for steady state fronts, but Hoskins and Heckley (1981) noted that this model is applicable only to cold fronts. In addition, numerical models with frontal propagation over a frictional boundary layer (Williams *et al.*, 1981; Hoskins and Heckley, 1981) have demonstrated that the frontal structure is relatively insensitive to the direction of propagation.

Williams *et al.* (1981) have suggested that warm fronts arise from horizontal deformations of the Bergeron (1928) type, and cold fronts from horizontal shear flows. However, as pointed out, for example, by Petterson (1956, p. 40 and 202), a shear motion is locally the sum of a pure deformation and a rotation, and the frontogenetic intensity of the horizontal flow is independent of its rotational component. Hence a shearing deformation is frontogenetically equivalent to a stretching deformation. Thus, the frontal structure should not be altered by the type of large-scale frontogenetic flow field.

Eliassen (1962) argued that differences in the longfront temperature variation of warm and cold fronts can account for their structural differences. By the thermal wind relation, the longfront temperature variation implies a geostrophic cross-front wind toward the cold air that decreases (increases) with height for cold (warm) fronts. Using the vertical circulation equation, Eliassen diagnosed that the ageostrophic deformation field would be more intense for cold fronts and would strengthen cold fronts relative to warm fronts. Gidel (1978) extended this argument by employing a two-dimensional numerical model of a front forced by a vertically sheared cross-front wind field. The simulated cold fronts are stronger, have a steeper tilt, and propagate faster than the simulated warm fronts. However, the model warm fronts developed in a frontolytic large-scale forcing.

An analysis of fronts formed in a semigeostrophic model of three-dimensional unstable baroclinic waves led Hoskins and Heckley (1981) to hypothesize that the forward tilt of the temperature wave with height accounts for the variations in frontal tilt and strength between warm and cold fronts. They supported this

idea with two-dimensional semigeostrophic simulations of fronts forced by an imposed horizontal deformation with prescribed tilts in the temperature field. The question of frontal propagation was not addressed.

The specific purpose of this study is to investigate the effects of the basic state static stability on frontogenesis. Beyond this limited objective, the results are believed to have more general relevance to the question of the distinction between warm and cold fronts.

Section 2 describes the semigeostrophic model in which an imposed stretching deformation forces a surface front in a semi-infinite Boussinesq atmosphere. Section 3 presents a comparison between two surface fronts formed with different basic state stratifications. Based on these results, a new hypothesis for the difference in warm and cold fronts is advanced in a concluding discussion section.

2. The model

Frontogenesis is forced by an imposed stretching deformation field independent of height whose horizontal streamfunction is $\psi = \alpha xy$. Here the atmosphere is a vertically semi-infinite Boussinesq rotating hydrostatic fluid in a Cartesian coordinate system (x, y, z) with constant Coriolis parameter $f > 0$ and gravity $-g\hat{z}$. The flat lower boundary lies at $z = 0$. The positive constant α measures the strength of the deformation in units of s^{-1}. Frontal formation is anticipated along the dilatation axis $x = 0$. The potential temperature field has the form

$$\theta(x, z, t) = T_{00} + \frac{d\theta_s}{dz} z + \theta_d(x, z, t), \qquad (1)$$

where $T_{00} = 278$ K is a reference temperature and $d\theta_s/dz$ is the constant basic state static stability. Taking the dynamic component θ_d to be independent of y restricts the analysis to straight infinitely-long fronts with no longfront variation.

This analysis follows the seminal work of Hoskins and Bretherton (1972). They show that for inviscid adiabatic flow with uniform potential vorticity the problem in the geostrophic coordinates, defined by

$$(x_s, z_s, t_s) \equiv (x + v/f, z, t), \qquad (2)$$

is identical to the quasi-geostrophic problem in physical space. Exact uniformity of the potential vorticity is achieved if θ_d is a harmonic function of x_s and Nz_s/f where $N = [(g/T_0)(d\theta_s/dz)]^{1/2}$ is the buoyancy frequency. A convenient initial condition is

$$\theta_d(x_s, z_s, 0) = \Delta\theta \tan^{-1}[x_s/(L + Nz_s/f)], \qquad (3)$$

where L is the characteristic horizontal length scale of the potential temperature field and $\Delta\theta$ is its magnitude. The solution for $t > 0$ is

$$\theta_d(x_s, z_s, t_s) = \Delta\theta \tan^{-1}(X/Z), \qquad (4)$$

where $X = x_s \exp(\alpha t)$ and $Z = L + Nz_s \exp(\alpha t)/f$. This result is readily obtained from (3.3) of Bannon (1983) by dropping the transient inhomogeneous contribution which reflects the nonuniformity of the potential vorticity in the standard quasi-geostrophic problem

$$\{\theta_d(x_s, z_s, 0) = \Delta\theta \tan^{-1}(x_s/L)\}.$$

That this term decays rapidly, like $\exp(-2\alpha t)$, indicates that (4) also is the asymptotic solution as $t \to \infty$ to the standard problem. The longfront velocity field associated with (4) is, from the thermal wind relation

$$f\partial v/\partial z_s = (g/T_0)(\partial\theta_d/\partial x_s),$$

$$v(x_s, z_s, t_s) = v_0 \ln[(X^2 + Z^2)/L^2 \exp(2\alpha t)], \qquad (5)$$

where $v_0 = g\Delta\theta/2NT_0$ and the constant of integration has been obtained as in Bannon (1983).

With v determined, the solution in physical space is obtained by making the inverse transformation numerically using Newton's method. The solutions are displayed graphically in the next section. Flow quantities are evaluated on a uniform grid in physical space with $\Delta x = 10$ km and $\Delta z = 100$ m.

3. Results

The salient effects of stratification on surface frontogenesis can be inferred by comparison of two model simulations with different values of the basic state static stability $d\theta_s/dz$. Figures 1 and 2 display the solutions with static stabilities of 4 and 2 K km^{-1}, respectively. They are referred to as the strong and weak stratification cases, respectively. An intermediate case with the typical atmospheric value of $d\theta_s/dz = 3$ K km^{-1} is not displayed, but its features are summarized quantitatively in Tables 1 and 2. These solutions correspond to the time $\alpha t = 0.90$ after the initial condition (3). In each case the parameter settings are $\Delta\theta = 30(2/\pi)$ K, $L = 10^3$ km, $g = 10$ m s^{-2}, $f = 10^{-4}$ s^{-1} and $T_0 = 300$ K. The only difference is the magnitude of the ambient stratification.

The three panels in each figure are patterned after Figs. 1, 3 and 2 of Blumen (1980). The general features of the model fronts are similar to those documented by Blumen, who compared theory with observations. The present simulations share the weaknesses noted by Blumen. However, it is beyond the scope of this paper to provide a detailed intercomparison between the two simulations or between the present simulations and observations. Rather, the role of stratification is examined by intracomparison of simulations using a single model.

A major result of this comparison is that the strength of the front, whether measured in terms of the inversion, vorticity or the thermal gradient, is greater for the weak stratification case. As noted by Hoskins and Bretherton (1972), a discontinuity develops when $\partial v/\partial x_s = f$. This critical time t_c is

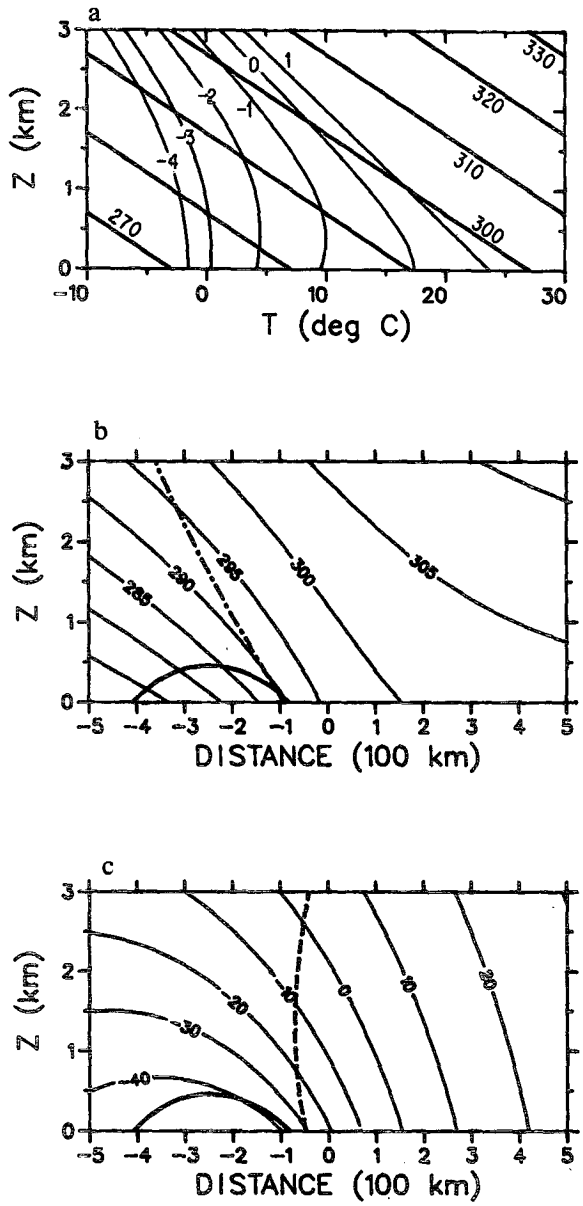

FIG. 1. Model front for a static stability of 4 K km^{-1}; the strong stratification case. (a) Temperature soundings at different distances from the surface inversion, labeled in units of 100 km. The heavy sloping straight lines are adiabats labeled in K. (b) The potential temperature field (K). (c) The longfront geostrophic velocity v (m s^{-1}). Positive values denote flow into the paper. Heavy solid curve in (b) and (c) is the inversion axis. Heavy dash-dot and dashed lines are the axes of maximum horizontal temperature gradient and maximum vertical vorticity, respectively.

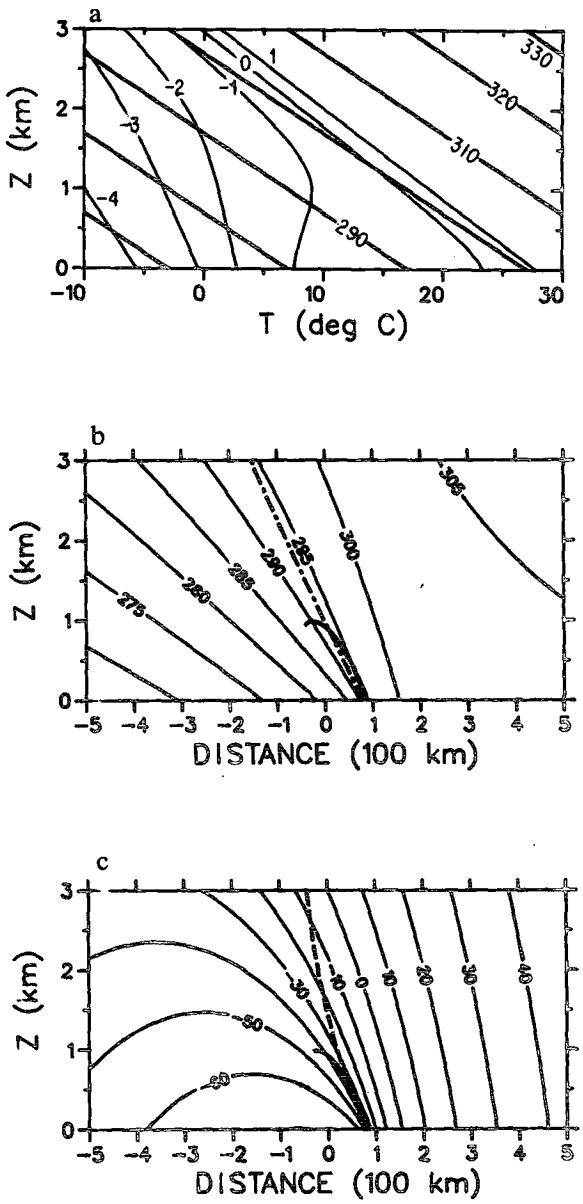

FIG. 2. As in Fig. 1, but for a static stability of 2 K km^{-1}; the weak stratification case.

$$\alpha t_c = \ln \frac{2NfLT_0}{g\Delta\theta}, \tag{6}$$

and increases logarithmically with the basic state static stability. Thus, though both fields have been exposed to the same large-scale forcing for equal periods of time, the weak stratification case is closer to the development of a discontinuity.

It is important to note that t_c is infinite for quasi-geostrophic theory. A reduction of t_c to finite values reflects the fact that semigeostrophic theory includes advection by the ageostrophic wind. Physically, the stable stratification tends to suppress the vertical circulation. Hence situations with large static stability lead to weak vertical deformations and concomitantly weak fronts.

It is convenient to introduce a nondimensional measure of the strength of the front, σ, defined by

$$\sigma \equiv \frac{g\Delta\theta \exp(\alpha t)}{2NfLT_0}. \tag{7}$$

TABLE 1. Stratification effects on frontal inversion.

Feature	Static stability (K km^{-1}) 2	3	4
Maximum temperature difference (K)	4.3	0.7	0.5
Displacement (km)	+88	−5	−81
Height (m)	988	482	452
Length (km)	118	204	328
Mean slope over first 100 km	1:108	1:213	1:253

Here σ is the maximum relative vorticity in geostrophic space, $\partial v/\partial x_s$, scaled by the planetary vorticity f. By (6), $\sigma = \exp[-\alpha(t_c - t)]$ and varies monotonically from zero in the quasi-geostrophic limit [$L \exp(-\alpha t) \to \infty$] to 1 at the time of formation of a discontinuity. Here $\sigma = 0.68$ (0.96) for the strong (weak) stratification case. The maximum relative vorticity is related to σ by

$$\left.\frac{1}{f}\frac{\partial v}{\partial x}\right|_{\max} = \frac{\sigma}{1-\sigma}, \tag{8}$$

and correspondingly varies from 0 to ∞.

The temperature soundings in Figs. 1a and 2a exhibit inversions and isothermal layers above the cold surface air. The maximum strength of the inversion is 0.5 (4.3) K for the strong (weak) stratification. The inversion axis, defined as the loci of points at the top of the inversion or the isothermal layer, is plotted as the heavy solid line in the lower panels of each figure. This axis extends horizontally for 328 (118) km over the cold air for the strong (weak) stratification.

It can be shown that the loci of points in geostrophic space associated with an isothermal region (i.e., $\partial T/\partial z = \partial\theta/\partial z - \Gamma = 0$) is given by

$$X = \left(\frac{\sigma L}{1-n^2}\right)[(1-2n^2) + r], \tag{9}$$

where

$$r = \pm\left[1 - \frac{(1-n^2)^2 Z^2}{\sigma^2 L^2}\right]^{1/2}. \tag{10}$$

Here $\Gamma = 10$ K km^{-1} is the dry adiabatic lapse rate and $n^2 = (d\theta_s/dz)/\Gamma$ is the ambient stratification scaled by Γ. The inversion axis in physical space is derived from (9) using the transformation (2). The positive root yields the portion of the inversion axis that starts near the maximum temperature gradient and slopes upward over the cold air. The negative root corresponds to a weak inversion ($\Delta T \leqslant 0.30$ K for Fig. 1) that extends downward into the cold air after the inversion has reached its maximum height. This unrealistic feature is evident in Figs. 1b and c. However, as the sounding 300 km behind the surface front (curve labeled −3 in Fig. 1a) indicates, the atmosphere in this region is essentially isothermal in the lowest 0.5 km. In addition, most of the solutions to (9) with a negative root for the weak stratification case are not associated with a surface inversion and are omitted in Figs. 2b and c.

The maximum height of the inversion, h_I, occurs for that value of z for which the radicand in (10) vanishes. One finds

$$h_I = \sigma L \exp(-\alpha t)\left(\frac{f}{N}\right)\left(\frac{1}{1-n^2} - \frac{1}{\sigma}\right). \tag{11}$$

The value of h_I varies from 458 m for the strong case ($n^2 = 0.4$) to 988 m for the weak ($n^2 = 0.2$) stratification case. In the quasi-geostrophic limit ($\sigma = 0$), $h_I < 0$ and no inversion exists. Inversions occur for $\sigma > 1 - n^2$.

The slope of the inversion is

$$\frac{\partial z}{\partial x} = -\left(\frac{f}{N}\right)\left(\frac{L}{Z}\right)\frac{\sigma}{1-n^2}\, rp, \tag{12}$$

where

$$p = \frac{(1-2n^2+2n^4) + (1-2n^2)r}{n^2 + (1-2n^2)r}.$$

Negative slopes, here and elsewhere, denote tilts over the cold air. The inversion slope at the ground is 1:174 (1:65) for the strong (weak) stratification case and decreases with height.

The potential temperature fields θ are displayed in the center panels of Figs. 1 and 2. The slope of the isentropes is steeper for the weak stratification of Fig. 2 than for the strong case of Fig. 1. In each case, most of the horizontal gradient lies in the cold air, and the gradient decreases with height. The maximum horizontal gradient, $[(\Delta\theta/L)\exp(\alpha t)]/(1-\sigma^2)$, is 8.7 (59.9) K (100 km)$^{-1}$ for the strong (weak) stratification.

The heavy dash-dot line denotes the axis of maximum horizontal temperature gradient (hereafter called the temperature gradient axis). This axis also tilts over the cold air (c.f. the quasi-geostrophic case in which the axis is vertical). Its equation is

$$x = \sigma L \exp(-\alpha t)\{1 - \ln[(\sigma^2 L^2 + Z^2)/L^2 \exp(2\alpha t)]\}. \tag{13}$$

TABLE 2. Stratification effects on temperature gradient and vorticity axes.

Feature	Static stability (K km^{-1}) 2	3	4
Temperature gradient axis:			
Maximum [K (100 km)$^{-1}$]	59.9	12.0	8.7
Displacement (km)	+79	−22	−90
Vorticity axis:			
Maximum (10^{-4} s^{-1})	24.0	3.6	2.1
Displacement (km)	+80	0	−46

The slope of the axis at the surface is

$$\left.\frac{\partial z}{\partial x}\right|_{z=0} = -\left(\frac{f}{N}\right)\left(\frac{1+\sigma^2}{2\sigma}\right), \tag{14}$$

and it has only a weak dependence on the stratification, being slightly less for the strong (1:100) than for the weak (1:90) stratification case. As σ increases from zero to 1, this slope varies monotonically from ∞ to (f/N).

The longfront geostrophic wind, shown in Figs. 1c and 2c, varies from −49.6 to 30.4 (−70.2 to 48.4) m s^{-1} for the strong (weak) stratification case. The maximum relative vorticity lies at the surface and is 2.1 (24.0) 10^{-4} s^{-1}. The heavy dashed line represents the axis of maximum cyclonic relative vorticity, hereafter called the vorticity axis. The equation for this axis is

$$x = \exp(-\alpha t)\{Z - \sigma L \ln[2Z^2/(L^2 \exp 2\alpha t)]\}. \tag{15}$$

Comparison of (13) and (15) indicates that for $\sigma < 1$ the vorticity axis lies on the warm air side of the potential axis. At $\sigma = 1$, the two axes coincide at the surface. The surface slope of the vorticity axis is

$$\left.\frac{\partial z}{\partial x}\right|_{z=0} = -\left(\frac{f}{N}\right)\left(\frac{1}{2\sigma - 1}\right). \tag{16}$$

Initially ($\sigma = 0$), the surface slope is positive and the axis tilts over the warm air. As the frontogenesis progresses, the axis rotates counterclockwise in the x–z plane to lie over the cold air. Figures 1c and 2c indicate that the rotation is more advanced in the weak stratification case (slope 1:75) compared to the strong stratification result (1:41). Equations (14) and (16) indicate that the surface slopes are identical when $\sigma = 1$. For the weak stratification case, this axis follows the inversion axis closely below 1.0 km, while that for the strong stratification case lies 44 km on the warm air side of the surface inversion and is essentially vertical aloft. Typically the vorticity axis is more vertical than the temperature gradient axis. The two axes more nearly coincide in the weak stratification case.

An important distinction between the weak and strong stratification solutions is the location of the intersection of the characteristic axes with the surface. The origin of the abscissa in Figs. 1b, c and 2b, c is the reference point x_r = 759 km which corresponds to the point of maximum cyclonic relative vorticity at the ground for the intermediate case $d\theta_s/dz$ = 3 K km^{-1}. The displacements in Tables 1 and 2 are measured relative to this point with positive (negative) values corresponding to shifts toward the warm (cold) air. Figure 1 reveals that the axes for the strong stratification case are displaced about 90 km on the cold side of the origin. (However, this still represents a net displacement of the front toward the warm air.) In contrast, the axes for the weak case are 90 km on the warm side. This behavior arises because the rate of frontal propagation is inversely proportional to the static stability. It can be shown that the location of the point of maximum surface temperature gradient propagates toward the warm air at speed v_F given by

$$v_F = \frac{\alpha g \Delta\theta}{N f T_0}\left(\frac{1}{1+\sigma^2}\right). \tag{17}$$

With $\alpha = 2 \times 10^{-5}$ s^{-1}, this speed is 11.0 (15.6) m s^{-1} initially ($\sigma = 0$) for the strong (weak) stratification case. At $\alpha t = 0.90$, these speeds have been reduced to 7.5 and 8.1 m s^{-1}, respectively. [Eq. (17) differs from the result of Bannon (1983, p. 2271) because (3) is used here. Moreover, the earlier result is for $\sigma = 0$. For $\sigma > 0$, the result is $x_m = X_m T[1 + 2\alpha t - \ln(1 + X_m^2)]$, where $X_m = -\epsilon(1 - T^2)/(\pi T S^{1/2})$ and $T = \exp(-\alpha t)$.]

Tables 1 and 2 summarize the major features of the simulations. In addition to the strong and weak stratification cases depicted in Figs. 1 and 2, the tables include the intermediate case $d\theta_s/dz$ = 3 K km^{-1}. Comparison of these results indicates the monotonic but nonlinear impact of variations in the static stability.

4. Discussion

A semigeostrophic model has been used to study the effect of stratification on surface frontogenesis. The only large-scale forcing present in the uniform potential vorticity model is a stretching deformation independent of height. The model has no surface friction, no longfront variation and no significant prescribed tilt of the thermal field.

The model results demonstrate that the ambient stratification significantly affects the structure and propagation characteristics of developing surface fronts. Specifically, model fronts forming in regions of large static stability are weaker, possess frontal inversions with a more gradual tilt, and propagate more slowly toward the warm air than fronts forming in regions of small static stability.

Physically these differences arise because the stratification modulates the intensity of the induced ageostrophic vertical deformation field. [By the Taylor–Proudman theorem, increases in the planetary vorticity can also help suppress the vertical motion field; this mechanism is reflected in (7) by the presence of f.]

The simulated variations in frontal strength and tilt are just those that distinguish warm fronts from cold fronts. The simulated variation in frontal propagation is also consistent with the warm/cold front distinction, provided that the appropriate uniform translation of the stretching deformation is included. [The semigeostrophic model is invariant to a Galilean transformation.] It should be noted that equal propagation speeds of warm and cold fronts toward the warm air will yield the occlusion process, but only if the cold front travels faster will it overtake the warm front, as is typically observed.

The preceding discussion holds for the case of a neutral occlusion. In the case of a cold-type occlusion, the cold front has a larger $\Delta\theta$ than the warm front and, by (17), will tend to propagate faster. This will enhance the ability of the cold front to overtake the warm front. The opposite effect holds for a warm-type occlusion.

These results suggest that the differences between warm and cold fronts arise from differences in their ambient static stability fields. In this theory, warm (cold) fronts are associated with strong (weak) stratification. In addition to the above considerations, this distinction agrees with the characteristic cloud forms of warm and cold fronts noted in the Introduction.

This hypothesis is consistent with that of Hoskins and Heckley (1981) and with the structure of growing baroclinic waves. Hoskins and Heckley emphasize the forward tilt of the temperature field with height in the wave. With warm fronts forming in advance of the warm sector, the thermal tilt produces increased static stability in the region of warm front formation (see Fig. 6 of Hoskins and Heckley). The converse holds for cold fronts. Since the perturbation static stability field is proportional to the geopotential height perturbation in quasi-geostrophic theory, the vertical phase structure of the perturbation static stability closely follows that of the height perturbation. Thus the typical location of warm (cold) front formation in a growing baroclinic wave has relatively strong (weak) stratification.

Hoskins and Heckley also impose a tilt in a two-dimensional deformation model to simulate cold and warm fronts, displayed in their Figs. 7b and c, respectively. Inspection of these figures indicates that the cold (warm) frontal simulation is associated with relatively weak (strong) stratification. This relation also holds for the cold front and warm front type A simulated in the growing baroclinic wave (compare their Figs. 4a and b). Again, the simulated distinction between cold and warm fronts is consistent with the present hypothesis.

It is important to note that the potential vorticity $q = (T_0/g)fN^2$ is different (though uniform) for the weak and strong stratification cases in this study. In contrast, Hoskins and Heckley simulate both cold and warm fronts in a single uniform potential vorticity flow. By (7), fronts of varying strengths can develop due to variations in the large-scale forcing α and/or in the initial thermal gradient $(\Delta\theta/L)$. However, it is unclear whether fronts of different strengths can develop in a uniform potential vorticity fluid for the same forcing and initial gradients. The present results suggest that this situation might arise when the induced vertical deformation field of one of the fronts is more strongly suppressed by a larger ambient stratification. In such a case the suppression of the vertical circulation would have to be relatively unaffected by the changes in the three-dimensional vorticity field and in the horizontal thermal gradients required to compensate the increased stratification and ensure uniform potential vorticity.

The results presented here emphasize the importance of the ambient static stability in modulating the structure, propagation and rate of intensification of developing fronts. Future theoretical research should examine this effect with more realistic frontal models. Observationally, statistical studies of the characteristics of warm and cold fronts and their ambient stratification are needed.

Acknowledgments. Financial support in part was provided jointly by the National Science Foundation and the National Oceanic and Atmospheric Administration under Grant ATM80-26790. Brian Hoskins and an anonymous reviewer made helpful comments on the manuscript.

REFERENCES

Ball, F. K., 1960: A theory of fronts in relation to surface stress. *Quart. J. Roy. Meteor. Soc.*, **86**, 51–66.

Bannon, P. R., 1983: Quasi-geostrophic frontogenesis over topography. *J. Atmos. Sci.*, **40**, 2266–2277.

Bergeron, T., 1928: Uber die dreidimensional verknupfende Wetteranalyse I. *Geofys. Publ.*, **5**, No. 6, 111 pp.

——, 1937: On the physics of fronts. *Bull. Amer. Meteor. Soc.*, **18**, 265–275.

Bjerknes, J., 1919: On the structure of moving cyclones. *Geofys. Publ.*, **1**, No. 2, 1–8.

——, and H. Solberg, 1921: Meteorological conditions for the formation of rain. *Geofys. Publ.*, **2**, No. 3, 60 pp.

——, and ——, 1922: Life cycle of cyclones and the polar front theory of atmospheric circulation. *Geofys. Publ.*, **3**, No. 1, 18 pp.

Blumen, W., 1980: A comparison between the Hoskins–Bretherton model of frontogenesis and the analysis of an intense surface frontal zone. *J. Atmos. Sci.*, **37**, 64–77.

Byers, H. R., 1974: *General Meteorology.* McGraw Hill, 461 pp.

Eliassen, A., 1962: On the vertical circulation in frontal zones. *Geofys. Publ.*, **24**, 147–160.

Gidel, L. T., 1978: Simulation of the differences and similarities of warm and cold surface frontogenesis. *J. Geophys. Res.*, **83**, 915–928.

Hoskins, B. J., and F. P. Bretherton, 1972: Atmospheric frontogenesis models: Mathematical formulation and solution. *J. Atmos. Sci.*, **29**, 11–37.

——, and W. A. Heckley, 1981: Cold and warm fronts in baroclinic waves. *Quart. J. Roy. Meteor. Soc.*, **107**, 79–90.

Houze, R. A., Jr., and P. V. Hobbs, 1982: Organization and structure of precipitating cloud systems. *Advances in Geophysics,* Vol. 24, Academic Press, 225–315.

Kutzbach, G., 1979: *The Thermal Theory of Cyclones. A History of Meteorological Thought in the Nineteenth Century.* Amer. Meteor. Soc., 254 pp.

Palmén, E., and C. W. Newton, 1969: *Atmospheric Circulation Systems.* Academic Press, 603 pp.

Petterson, S., 1956: *Weather Analysis and Forecasting, Vol. 1.* McGraw Hill, 428 pp.

Williams, R. T., L. C. Chou and C. J. Cornelius, 1981: Effects of condensation and surface motion on the structure of steady-state fronts. *J. Atmos. Sci.*, **38**, 2365–2376.